Nano Energy 46 (2018) 257–265

Contents lists available at ScienceDirect

Nano Energy

journal homepage: www.elsevier.com/locate/nanoen

Full paper

Hue tunable, high color saturation and high-efficiency graphene/silicon heterojunction solar cells with MgF_2/ZnS double anti-reflection layer

Ke Ding[a], Xiujuan Zhang[a], Ling Ning[a], Zhibin Shao[a], Peng Xiao[a], Anita Ho-Baillie[b], Xiaohong Zhang[a], Jiansheng Jie[a,*]

[a] Institute of Functional Nano & Soft Materials (FUNSOM), Jiangsu Key Laboratory for Carbon-Based Functional Materials & Devices, Soochow University, Suzhou 215123, Jiangsu, PR China

[b] School of Photovoltaic and Renewable Energy Engineering, University of New South Wales, Sydney, NSW 2052, Australia

ARTICLE INFO

Keywords:
Graphene/silicon solar cells
Multi-color
Hue tunable
MgF_2/ZnS double anti-reflection layer

ABSTRACT

Graphene/silicon (Gr/Si) heterojunctions with simple manufacturing process, high stability and excellent device performance have great potential in photovoltaic (PV) applications. In comparison to conventional PV panels with monotone colors, multi-color PV panels could be integrated in modern building facades and thus largely expand their application ranges. In this work, multi-color Gr/Si heterojunction PV devices were fabricated, for the first time, by taking advantage of the combination of ultra-thin highly transparent graphene and MgF_2/ZnS anti-reflection coating. The double-layer film coating enabled the multi-color Gr/Si PV devices with both high color saturation and low optical loss. The PV devices exhibited respectable power conversion efficiency (PCE) in the range of 10.7–13.2%, depending on the color of the devices. In addition, PCE of the device with optimized anti-reflection coating reached as high as 14.6%, which is among the highest for the Gr/Si heterojunction solar cells. By varying the film thickness at different positions, a colored Gr/Si solar cell with visible pattern was made on a 2-in. Si wafer. Our work demonstrates the great potential of multi-colored Gr/Si solar cells for new-generation distributed solar energy systems with designable features.

1. Introduction

To expand the applications of photovoltaics beyond rooftops and solar farms, aesthetically pleasing solar modules such as colored modules can find applications in building-integrated photovoltaic (BIPV) systems which form part of the building fabric as well as generate electrical energy simultaneously [1]. There are various approaches to achieve color solar cells. The first method is to utilize the intrinsic colors of the active layers in PV devices. The active layers of organic photovoltaics (OPVs) [2], dye sensitization solar cells (DSSCs) [3] and organic-inorganic hybrid perovskite solar cells [4] can produce different color appearance. In these devices, the colors are mainly determined by the energy band structures of the active layers and are difficult to be tuned. Only a few colors could be realized and the performance of bright-color devices is poor in general. Another method is to utilize coherent interference of incident light to realize structural color, such as using sub-wavelength photonic crystal structures [5–8] and thin dielectric film stacks [9]. The thin dielectric film stacks are especially suitable for silicon (Si)-based solar cells owing to simple preparation processes. The high reflective strength (about 40% uniformly in visible (VIS) range) of Si offers an excellent condition to easily construct hue tunable solar cells *via* light interference [10–13]. As a contrast, the color-tunable perovskite solar cells, which have a lower light reflectivity, need a complicated SiO_2 photonic crystal/TiO_2 multilayer thin film stack as high reflective "mirror" to achieve the color-tunable characteristics [14]. Since the composite film served as charge collecting layer at the meantime, the layer thickness strongly affected the charge transport and resulted in inferior device performance at different colors. Although Si-based solar cells offer better color tuning, the requirement for thick transparent conductive electrode or surface passivation layer in conventional Si-based solar cells, including Si p-n junction [15], Si heterojunction [16], and organic-Si hybrid solar cells [17], still limits the color tuning range as well as the color purity. This is because of the mismatched reflective indices between these layers with Si and their light absorption in VIS range.

In contrast, in graphene/silicon (Gr/Si) heterojunction solar cells, the graphene layer is almost negligible for structural color due to its ultrathin thickness (0.34 nm) and high transparent characters (97.7%). Also, a molecular surface modification layer or an ultrathin oxidation layer was often used in the Gr/Si heterojunction solar cells [18,19],

* Corresponding author.
E-mail address: jsjie@suda.edu.cn (J. Jie).

https://doi.org/10.1016/j.nanoen.2018.02.005
Received 27 November 2017; Received in revised form 19 January 2018; Accepted 1 February 2018
Available online 05 February 2018

thus avoiding the influence of thick surface passivation layers. In this regard, Gr/Si heterojunction is an outstanding platform to investigate and realize high-color-purity, high-performance multi-color PV devices. Gr/Si heterojunctions have been intensively studied in the past few years [20–32]. For instance, Li et al. first reported Gr/Si solar cells with a power conversion efficiency (PCE) of about 1.5% [33]. Xie et al. improved the device performance to 10.4% by enhancing light absorption with Si micro-holes and the graphene conductivity with $AuCl_3$ modification [34]. Gr/Si solar cells with PCE of 14.5% were achieved by Shi et al. through the coating of TiO_2 anti-reflection layer [35]. In despite of the large progress, the monotonous dark appearance of the Gr/Si heterojunction solar cells has no obvious change to conventional Si solar cells.

Herein, we report, for the first time, the fabrication of multi-color Gr/Si heterojunction solar cells by using double-layer (DL)-MgF_2/ZnS stack as the anti-reflection layer. This strategy has several important advantages: (i) In Gr/Si solar cells, the influence of transparent conductive electrode and surface passivation layer on structural colors could be neglected, thus offering a higher freedom to tune the device color. (ii) The use of DL-MgF_2/ZnS renders parasitic reflection in VIS region, yielding a sharp reflection peak with high-purity structural color. Moreover, the structural color could be readily tuned by varying the film thickness. (iii) The resultant multi-color Gr/Si solar cells exhibit high color purity as well as excellent device performance. The PCEs of multi-color Gr/Si devices (effective device area of 0.07 cm^2) with DL-MgF_2/ZnS coating are in the range 10.7–13.2%, and the highest efficiency of 14.6% is achieved if the DL film is used as an optimized anti-reflection coating. Given the high efficiency and high color purity, the multi-color Gr/Si heterojunction solar cells will have important applications in diverse fields, such as BIPV systems.

2. Experimental section

2.1. Optical simulation

FDTD method (FDTD Solutions, Lumerical) was used to simulate the optical absorption and reflection of devices. Fig. S2 illustrates the simulation model. The material dates of Si and graphene came from the material library of the software. SiN_x was regarded as a non-dispersive n-k (n = 2.0, k = 0) material to simulate optical film with 2.0 reflective index. The optical properties of MgF_2 and ZnS were referred from the website of http://refractiveindex.info (MgF_2: Dodge 1984: n(e) 0.2–7.0 μm, ZnS: Querry 1987: n, k 0.220–167 μm). Graphene is different from most optical materials owing to the ultrathin layer and thus is characterized using a surface conductivity model. A planer wave light source with 350–1400 nm wavelength was deployed over the device. The power density distribution monitor was set on light source to record the reflectivity of device. Boundary conditions of XZ and YZ planes were periodic boundary conditions to simulate extensibility of Si wafer. On the other hand, the perfectly matched layer (PML) boundary condition was set on XY plane to absorb arrived light.

2.2. Synthesis and transfer of graphene film

Graphene were prepared at 1000 °C by using a mixed gas of CH_4 (40 sccm) and H_2 (20 sccm) *via* chemical vapor deposition (CVD). Cu foil with 25 μm thickness was used as the catalytic substrate. The as-prepared graphene film was spin-coated with 8 wt% polymethyl-methacrylate (PMMA), and then the underlying Cu substrate was etched away in ferric chloride solution ($FeCl_3{\cdot}6H_2O$: H_2O = 50 g: 50 mL). The PMMA-supported monolayer graphene was ready to transfer onto Si substrate.

2.3. Device construction and evaluation

To construct the Gr/Si heterojunction solar cells, n-type Si substrates (orientation < 100 > , resistivity 1–3 Ω cm) with 300 nm thick SiO_2 dielectric layers were first protected by adhesive tapes with opening windows of 0.07 cm^2 or 1 cm^2, which defined the work areas of the devices. Then the SiO_2 layers within the window areas were removed by 5% HF solution. Afterwards, in order to suppress the surface carrier recombination, the Si wafer was further functionalized with monolayer methyl groups *via* a two-step chlorination/alkylation method according to previous reports [18,36–40]. The cleaned PMMA-supported monolayer graphene layer was then transferred onto the substrates and dried naturally. The size of graphene layer was a little larger than the junction area to ensure a good contact of graphene layer with the metal electrode pre-deposited on SiO_2 insulator layer. Indium-Gallium (In-Ga) alloy was pasted on rear side of Si wafer as the ohmic contact. To improve the conductivity of graphene layer in large-area devices, Ag grid mesh was fabricated on Gr/Si heterojunctions by photolithography and thermal evaporation. Photolithography was conducted on a mask aligner (SUSS-Micro Tec, MJB4) by using positive photoresist (AR-P 5350, Allresist). Eventually, ZnS (Strem Chemicals, 99.99%) and MgF_2 (Alfa Aesar, Optical Grade, 99.9%) films were deposited in sequence onto the Gr/Si heterojunctions by thermal evaporation to generate the structural colors. The deposition rate as well as film thickness were monitored by quartz crystals oscillator.

Morphology of the metal grid mesh was investigated by scanning electron microscope (SEM, FEI Quanta 200FEG). Reflection spectra were measured by a spectrometer (Perkin-Elmer Lambda 750) equipped with an integrating sphere. The film thickness was determined by a spectroscopic ellipsometer (J.A. Woollam, Alpha-SE). Photovoltaic characteristics of the solar cells were evaluated by using a Keithley 2612 source meter in an ambient environment. A Newport 91160 solar simulator equipped with a 300 W xenon lamp and an AM 1.5 filter was used to generate simulated AM 1.5 solar irradiation (100 mW/cm^2).

3. Results and discussion

In this work, DL-MgF_2/ZnS films were used to achieve high-saturation colors for Gr/Si heterojunction solar cells. ZnS nearly owns the maximum refractive index (n = 2.5) while MgF_2 owns the minimum refractive index (n = 1.4) in solid transparent materials (for Si solar cells, from 380 to 1100 nm). Therefore, the DL-MgF_2/ZnS films could serve as efficient antireflection layers for Si solar cells. Meanwhile, they have appropriate refractive index difference, making them suitable to produce high-saturation colors for Gr/Si heterojunction solar cells. Fig. 1a displays the schematic illustration of device structure. The device was fabricated on a SiO_2/n-Si substrate with an opened Si window (1 × 1 cm^2). Graphene layer was transferred onto the window to form the heterojunction. Ag mesh grids were deposited on the graphene as the front electrode, while In-Ga eutectic alloy was painted on the rear side of Si wafer as back electrode. Finally, the ZnS and MgF_2 films were thermally evaporated onto the front. Their thickness was controlled to achieve different structural colors. Fig. 1b shows the photographs of Gr/Si heterojunction solar cells with seven rainbow colors. The coordinates of seven colors in Commission Internationale de L'Eclairage (CIE) chromaticity are demonstrated in Fig. 1c. The chromaticity coordinate positions are close to the edges of graph, indicating high-saturation colors realized by the DL-MgF_2/ZnS films.

Note that the use of DL-MgF_2/ZnS films is crucial to achieve the high-saturation colors for the Gr/Si solar cells. In a control experiment, the hues transform with the use of single layer (SL)-ZnS was also investigated, as shown in Fig. 2. It is observed that the existence of graphene layer on the top of Si substrate has no impact on the structural colors (Fig. S1). Therefore, to simplify the analysis, we removed graphene layer in the system for the following optical simulation. Fig. 2a shows the reflective spectra of uncoated Si wafer and ZnS-coated Si wafer with varied thickness of 60, 130 and 260 nm, respectively with evidence of optical interference. The minimum intensity of the reflective spectrum is called destructive interference valley (DIV). Film thickness H and refractive index n determine the wavelength position of

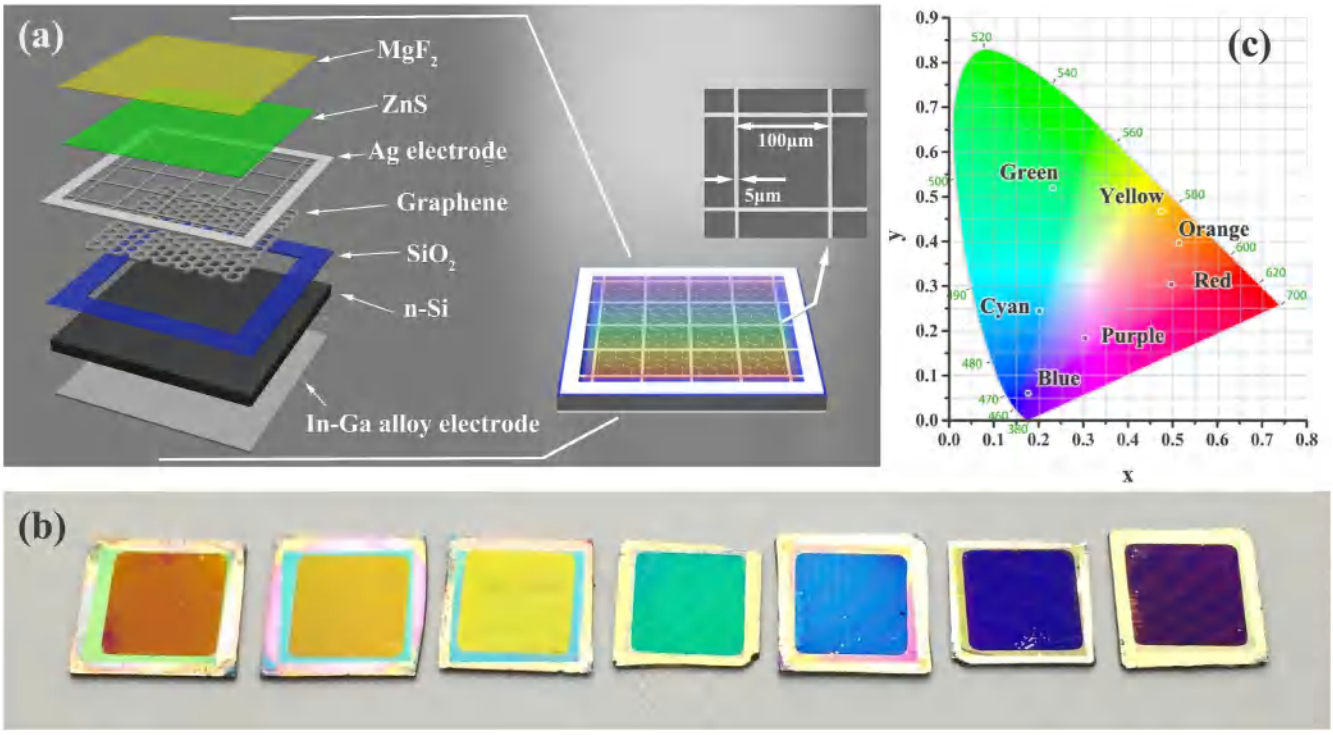

Fig. 1. (a) Schematic illustration of color Gr/Si heterojunction solar cells with DL-MgF_2/ZnS films. Inset shows the SEM image of the Ag grid mesh. (b) Photographs of Gr/Si heterojunction solar cells (device area: 1 cm^2) with different colors. (c) Coordinates of seven colors in CIE chromaticity. The high color saturation is reflected by the coordinate positions that are near the edges.

DIV:

$$\lambda_{DIV} = \frac{4nH}{2k+1} \quad (k = 0,\ 1,\ 2...) \tag{1}$$

where k is the DIV order. Similarly, the maximum intensity caused by constructive interference is called constructive interference peak (CIP). The wavelength position of CIP has the following relationship with H and n:

$$\lambda_{CIP} = \frac{2nH}{k}(k = 1,\ 2...) \tag{2}$$

Since there will be more than one DIV or CIP in the reflection spectrum, we set DIV_k [material, H] and CIP_k [material, H] as symbols to describe the valleys and peaks, respectively, under different materials and film thickness. It is obvious that the wavelength positions of CIPs in VIS determine the structural colors, while the widths and number of CIPs are highly related with the color purity and absorption of solar cells. The fewer the CIPs and the sharper the CIPs in VIS, the purer the color and the higher the light absorption in Si wafer. We stimulated the reflective spectra of ZnS-coated Si wafer with different ZnS film thickness, as show in Fig. 2a. The detailed simulation model is shown in Fig. S2. The yellow curve depicts the reflective spectrum of 60 nm-ZnS coated Si wafer, which demonstrates a wide DIV (denoted by DIV_0 [ZnS, 60]) in VIS and near-infrared (NIR) region. So, this film is suitable to act as an excellent anti-reflection coating. In this case, the wavelength position of CIP_1 [ZnS, 60] is lower than 400 nm, thus reflecting blue or purple color, a common color found for Si p-n junction solar cells in the market. As we increase the ZnS thickness to 130 nm (orange curve in Fig. 2a), a wide reflection band could be observed in VIS and NIR range. The CIP_1 [ZnS, 130] at ~ 620 nm delivers a yellow structural color. However, the CIP_1 [ZnS, 130] spans from 450 to 1200 nm with a width of ~ 750 nm. The strong light reflection will

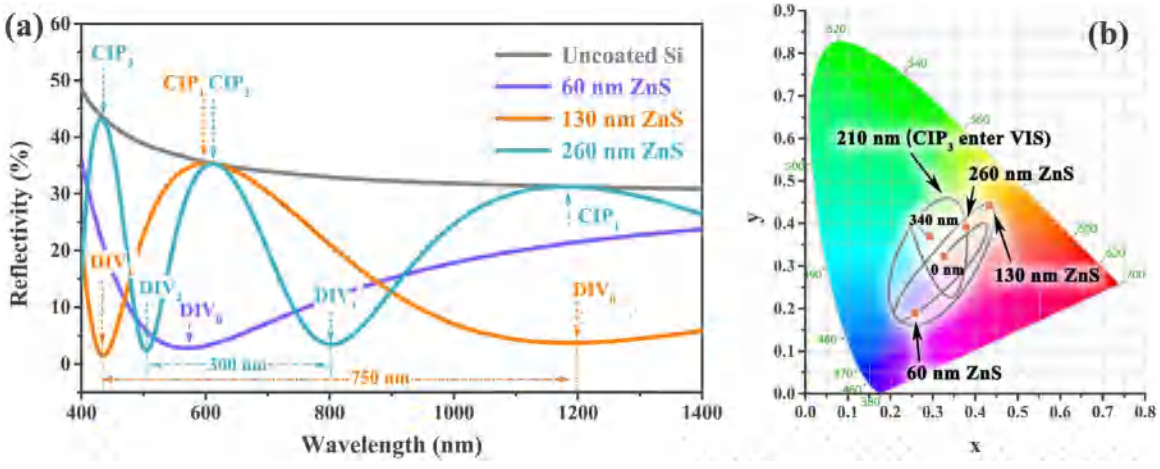

Fig. 2. (a) Reflective spectra of Si wafer with 0, 60, 130, and 260 nm thick SL-ZnS. (b) Structural colors variation with increasing SL-ZnS thickness.

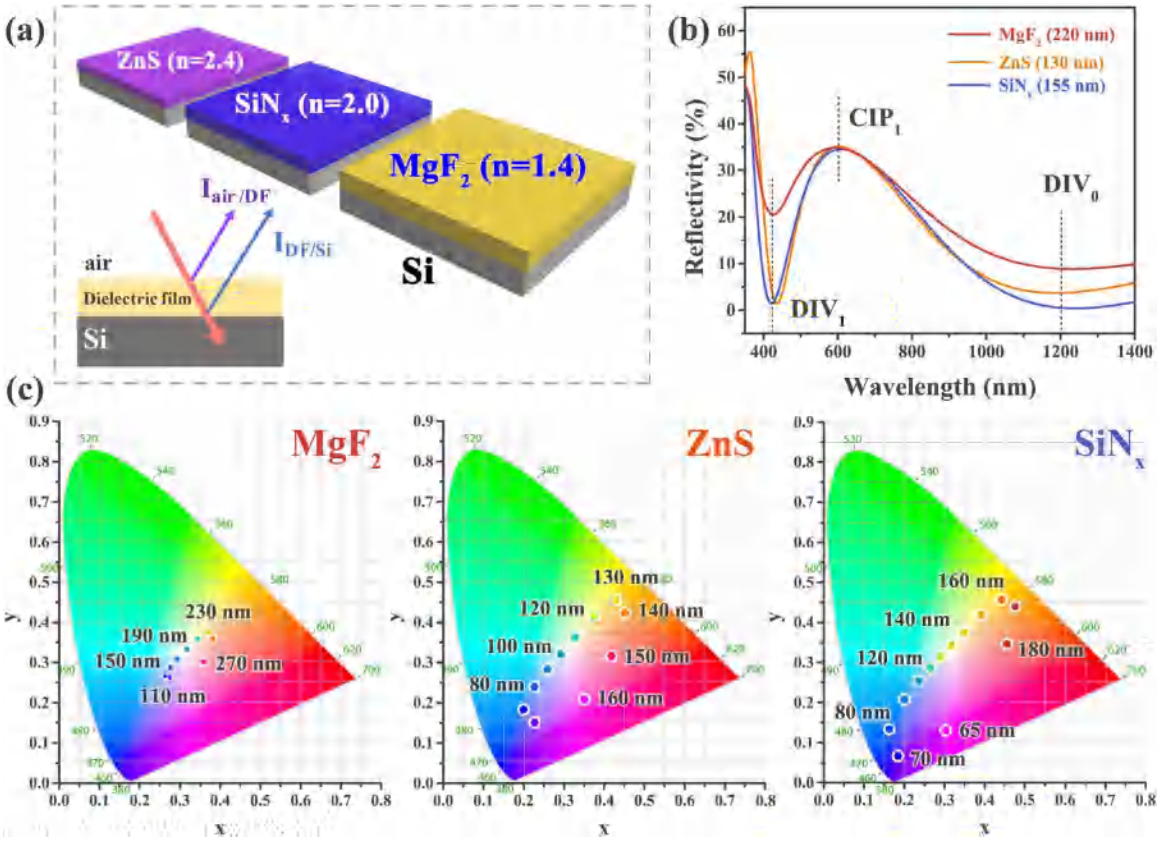

Fig. 3. (a) Schematic illustrations of SL-ZnS, SL-SiN_x and SL-MgF_2 coated Si wafers. Inset at the lower left shows intervene rays reflected from the two interfaces: air/DF and DF/Si. (b) Simulated reflective spectra of Si wafers coated with 220 nm MgF_2, 130 nm ZnS and 155 nm SiN_x, respectively. The optical path lengths in these three cases were retained to be the same by controlling the film thickness. (c) Coordinates variation (CIP_1 in VIS region) with increasing thickness for three different materials.

remarkably reduce the Si absorption and thus degrade the performance of solar cells. Compared with the yellow color in Fig. 1c with DL-MgF_2/ZnS film coating, the structural color of 130 nm SL-ZnS-coated Si wafer is closer to the write point (center of CIE chromaticity), indicating an inferior color purity. Further increasing the SL-ZnS film to 260 nm demonstrates a narrower CIP_2 [ZnS, 260] at 620 nm (cyan curve in Fig. 2a). However, the appearance of additional CIPs of CIP_1 [ZnS, 260] and CIP_3 [ZnS, 260] in VIS and NIR range reduces color purity and lowers light absorption (Fig. 2b). From Fig. 2b, it is observed that, as the SL-ZnS film thickness increases, the color shows a periodical change from purple to red when film thickness is lower than 210 nm. However, when the thickness is beyond 210 nm, more than one CIP will appear in VIS region, leading to an unpredictable mixed color effect and always with reduced color purity. Therefore, it is hard to realize high color purity and low light reflection at the same time by simply tuning the thickness of the SL film.

Besides the film thickness, the refractive index n is another important parameter for SL film to determine its reflective properties. As Fig. 3a shows, three kinds of dielectric films (DFs) with different n values, ZnS (n = 2.4), SiN_x (n = 2.0) and MgF_2 (n = 1.4), were selected to study the relationship between n and structural colors. The inset in Fig. 3a shows the intervene rays reflected from two interfaces: air/DF and DF/Si. Different film thicknesses of ZnS (130 nm), SiN_x (155 nm) and MgF_2 (220 nm) were used to ensure the optical path lengths $\Delta = 2nH$ in DFs for the rays reflected at DF/Si interfaces are almost the same. Therefore, the CIPs and DIVs for these three systems have the same positions (CIP_1 at 620 nm, DIV_0 at 1200 nm and DIV_1 at 410 nm). In spite of this, the reflective intensities of DIVs in these three systems are quite different as shown in Fig. 3b. MgF_2/Si and ZnS/Si show much higher DIVs compared to SiN_x/Si. Since the reflective intensities of DIVs are directly related with the color purity and light absorption of the system, the SiN_x/Si exhibits purer colors (Fig. 3c) than MgF_2/Si and ZnS/Si due to less parasitic reflection near the DIVs. This result could be understood by the following equation:

$$I = \frac{(n_1 - n_2)^2}{(n_1 + n_2)^2} \quad (3)$$

where I is the reflect intensity on optical interface, and n_1 and n_2 represent the reflective index of the two sides' materials at the optical interface. Based on this equation, only if $I_{air/DF} = I_{DF/Si}$, "zero reflection" come into being for DIVs due to opposite phase and same reflective intensity. Owing to the right n value of 2.0, SiN_x becomes a perfectly matched material between Si (n = 4.0) and air (n = 1.0). The almost equal $I_{air/SiNx}$ and $I_{SiNx/Si}$ lead to minimum reflective intensity for DIVs. In contrast, n values for ZnS (2.4) and MgF_2 (1.4) deviate from the ideal value (n = 2.0), thus resulting in redundant light reflection at DIVs. Although the use of SiN_x with suitable n value could enhance the color saturation and reduce the light reflection to some extent, the huge span of CIP_1 from VIS to NIR restricts color purity and device performance based on SL film. In principle, if the higher order CIPs (such as CIP_2 instead of CIP_1), could be used as the peak in VIS for color development without the appearance of mixed color effect and strong NIR reflection, the color purity and device performance could be remarkably improved.

In this work, DL-MgF_2/ZnS films were introduced to make use of CIP_2 as the peak for color development, while retaining the minimum parasitic reflection by other CIPs. Fig. 4a shows the film structures and the structural colors for both SL-ZnS and DL-MgF_2/ZnS coated Si wafers. Note that the device based on DL-MgF_2/ZnS (220 nm/130 nm) possesses high-saturation yellow color, in contrast to the low-saturation yellow color for the device based on 130 nm SL-ZnS and green shifted yellow color for the device based on 260 nm SL-ZnS. Fig. 4b depicts the

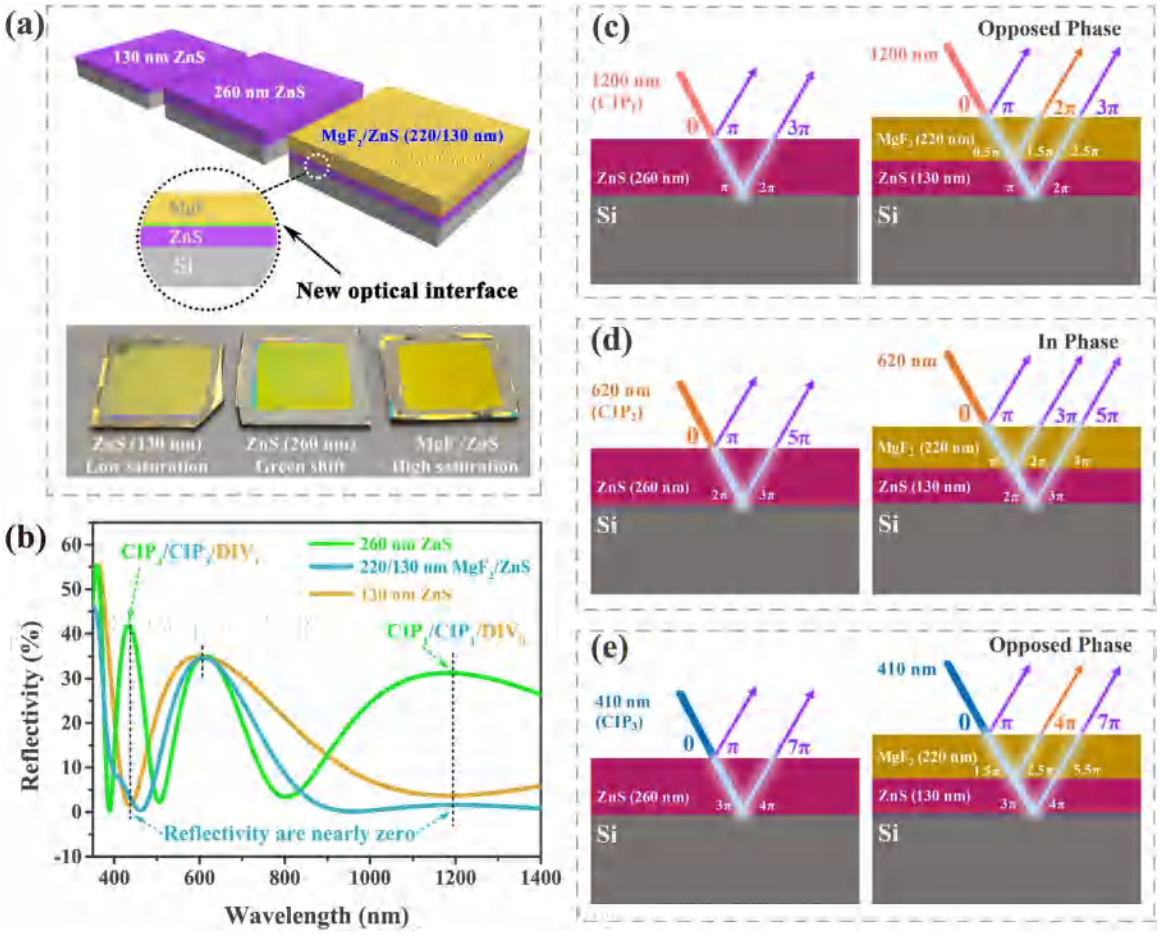

Fig. 4. (a) Schematic illustration of DL-MgF_2/ZnS on Si wafer, the new optical interface between ZnS and MgF_2 effectively tunes the film interference. Inset at the bottom shows the photographs of the SL-film-coated and DL-film-coated Si wafers, respectively. The 130 nm-ZnS-coated device shows low color saturation. 260 nm-ZnS-coated device shows color shift because another CIP (CIP_3) enters into VIS region. DL-MgF_2/ZnS (220 nm/130 nm)-coated device exhibits much higher color saturation. (b) Simulated reflective spectra of Si wafers with 130 nm SL-ZnS, 260 nm SL-ZnS and DL-MgF_2/ZnS (220 nm/130 nm) coating, respectively. (c-e) Phases of intervene rays reflected at the optical interfaces of ZnS/Si and MgF_2/ZnS/Si under different incident wavelengths of (c) 1200 nm (CIP_1), (d) 620 nm (CIP_2) and (e) 410 nm (CIP_3), respectively. (Note that the light rays showing incidence at a given angle in Fig. 4c-d only visually describe the interference process in thin films. In fact, we merely discuss the cases of normal incidence in this paper.).

corresponding reflective spectra. Significantly, the width for CIP_2 [MgF_2/ZnS, 220/130] in VIS region has been significantly reduced to be about 400 nm, which is much sharper than the CIP_1 [ZnS, 130]. Although the peak for DL film is a little bit wider than the CIP_2 [ZnS, 260], no other CIPs appear in VIS and NIR region (compared to 260 nm SL-ZnS). This is due to the generation of new optical interface between ZnS and MgF_2. 130 nm ZnS and 220 nm MgF_2 possess nearly consistent optical paths, and likewise optical paths of 260 nm SL-ZnS and the DL-MgF_2/ZnS (220 nm/130 nm) films are almost the same. Therefore, they have the same wavelength positions for CIPs with CIP_1 at 1200 nm, CIP_2 at 620 nm and CIP_3 at 410 nm (Fig. 4b). Fig. 4c-e show the phase analysis for the light reflection at different optical interfaces. Light phases of the CIP rays reflected from air/ZnS and ZnS/Si interfaces in ZnS/Si are the same (2π or integral multiple of 2π) (left sides of Fig. 4c–e), which means a constructive interference for all the wavelengths. In contrast, for DL-MgF_2/ZnS coated Si wafer, as shown in the right sides of Fig. 4c–e, only CIP_2 (620 nm) has the same light phases for the light rays reflected from different optical interfaces and shows constructive interference. Both CIP_1 and CIP_3 possess opposite phases between the reflective light rays from the new optical interface (MgF_2/ZnS) and other two interfaces (air/MgF_2 and ZnS/Si), leading to destructive interferences. “Zero reflection” for CIP_1 and CIP_3 could even appear when the reflective intensity from MgF_2/ZnS interface equals to the sum of reflective intensities from air/MgF_2 and ZnS/Si interfaces. As we have mentioned above, the reflective intensity depends on the reflective index of dielectric materials. By simulating different DL systems (MgF_2/ZnS, MgF_2/SiN_x and SiN_x/ZnS) in Fig. S3, we found MgF_2/ZnS is the best producing lowest reflection at CIP_1 and CIP_3. The reflection intensity at MgF_2/ZnS interface ($I_{MgF2/ZnS}$) is about 8.0%, which is nearly equal to the sum of $I_{air/MgF2}$ and $I_{ZnS/Si}$ (2.7% + 5.3% = 8.0%) (if we do not consider refractive index dispersion, oblique incidence and incident light loss in DFs), resulting in a nearly “zero reflection” at CIP_1 and CIP_3. Given the narrow CIP in VIS light and wide “zero reflection” region in Si absorbable spectral regime, the DL-MgF_2/ZnS-based structural colors will have great potential for multi-color, high-performance solar cells with vivid color appearance.

The multi-color Gr/Si heterojunction solar cells were fabricated by carefully tuning the thickness of DL-MgF_2/ZnS films. Table 1 lists the thickness of DL-MgF_2/ZnS films for achieving different structural colors. Note that, as the saturation of green color is relatively poor under normal thickness, we doubled the films' thicknesses for green-color device to achieve higher color saturation (Fig. S4). Also, devices with smaller effective areas of 0.07 cm^2 were measured to eliminate the influence of graphene conductivity on device performance. Thanks to the outstanding transmittance of graphene, the measured reflection spectra (solid lines in Fig. 5a) are in good agreement with the finite-different time-domain (FDTD) simulated results (dash lines in Fig. 5a), although small deviations caused by imperfect film quality can be observed. Moreover, the external quantum efficiency (EQE) spectra of these devices show similar trends to reflection spectra (Fig. 5b).

Table 1
Device parameters of color solar cells (device area 0.07 cm^2) with DL-MgF_2/ZnS coating.

Color	ZnS thickness (nm)	MgF_2 thickness (nm)	J_{SC} (mA/cm^2)		V_{OC} (V)	FF	PCE (%)
			Measurement	Integration of EQE			
Uncoated Si	0	0	23.0	23.2	0.55	0.67	8.5
Red	150	250	28.1	28.3	0.57	0.67	10.7
Orange	140	240	29.9	30.2	0.56	0.69	11.5
Yellow	130	220	30.0	30.1	0.58	0.68	11.9
Green	220	380	30.9	30.5	0.57	0.68	11.8
Cyan	90	170	31.9	31.6	0.55	0.68	12.0
Blue	70	130	33.7	33.8	0.57	0.67	12.8
Purple	60	120	34.5	34.2	0.57	0.67	13.2
Dark	55	100	35.6	35.3	0.57	0.72	14.6

Obviously, the uncoated Gr/Si solar cell shows the lowest EQE value, around 50% in the visible range. In contrast, an optimized DL-MgF_2/ZnS (100 nm/55 nm) anti-reflection coating greatly enhances the light absorption, resulting in high EQE exceeding 90% in the VIS range. In this case, the Gr/Si device has a dark appearance due to very low reflection (Fig. S5). As for the multi-color devices, there are optical losses due to reflections. However, their light absorptions are still much higher than that of the uncoated devices. As a result, they have EQEs between those of the optimized-film-coated devices and that of the uncoated device.

Fig. 5c shows the current density *versus* voltage (*J-V*) curves of the devices with different structural colors, and the corresponding photovoltaic parameters are summarized in Table 1. We note that the fill factor (FF) and open circuit voltage (V_{OC}) of the devices are very similar. However, the devices with cool color tone generally exhibit higher short circuit current densities (J_{SC}) than devices with warm color tone, due to the wider CIP with film thickness increasing. Compared with uncoated Gr/Si solar cell, which has poor J_{SC} (23.0 mA/cm^2) and PCE (8.5%) due to the weak light harvesting, the color solar cells have largely improved J_{SC} and PCE because of the effectiveness of DL-MgF_2/ZnS stack with gradient reflective index as an anti-reflection coating. Significantly, a high PCE of 10.7–13.2% can generally be achieved for the multi-color Gr/Si solar cells. Moreover, under the optimized DL-MgF_2/ZnS (100 nm/55 nm) anti-reflection coating, the dark-color device shows very low optical loss with J_{SC} of 35.6 mA/cm^2, V_{OC} of 0.57 V and FF of 0.72, yielding a high PCE of 14.6%. This value is among the highest for the Gr/Si heterojunction solar cells.

Compared to the SL-ZnS-coated devices, the DL-MgF_2/ZnS-coated multi-color devices show obvious advantages in color purity and device performance. Fig. 5d shows the photovoltaic performance of Gr/Si heterojunction solar cells with SL-ZnS (130 nm) and DL-MgF_2/ZnS (220 nm/130 nm) coating. Although both of the devices have yellow color, the J_{SC} and PCE increase remarkably from 28.1 mA/cm^2, 10.6% for SL-ZnS-coated device to 30.0 mA/cm^2, 11.9% for DL-MgF_2/ZnS-coated device. We note that the devices with other colors also show the similar results (Table S1, Table S2 and Fig. S6) Meanwhile, the color purity has been significant increased when using DL-MgF_2/ZnS coating. Fig. 5e displays the chromaticity coordinates of the Gr/Si solar cells with seven different colors upon the use of SL-ZnS (triangular) and DL-MgF_2/ZnS (circle) coating, respectively. The detailed color coordinates are shown in Table S3. In comparison with the SL-ZnS-coated devices, the coordinate points for DL-MgF_2/ZnS-coated devices move obviously toward the edges of chromaticity diagram, manifesting a much higher color purity. Therefore, the DL-MgF_2/ZnS-coated multi-color Gr/Si heterojunction solar cells possess the advantages of both high PV performance and high color purity.

Besides the small-area devices, the Gr/Si heterojunction solar cells with a large area of 1 cm^2 were also studied. The device area of 1 cm^2 is often regarded as a criterion for the large-size device in laboratory. In previous work, 1 cm^2 Gr/Si usually showed very poor PCE below 5% [18], due to the relatively low conductivity of graphene. Therefore, in this work, we fabricated Ag grid mesh with 96% duty cycle by photolithography on the top of graphene layer. The Ag grid mesh used in this work significantly reduces the sheet resistance of graphene from ~ 1000 Ω/ϒ to ~ 10 Ω/ϒ without any optical effect due to the small width (5 μm) and large spacing (100 μm). Fig. 5f depicts the *J-V* curves of the 1 cm^2 multi-color Gr/Si devices, and the detail PV parameters are summarized in Table S4. Compared with the small-area devices, J_{SC} of 1 cm^2 devices are similar to those of smaller devices under the same colors, showing negligible impact from metal grid mesh on light reflection and absorption. Nevertheless, V_{OC} and FF drop a bit for the 1 cm^2 devices due to the leakage current caused by partial contact of Ag mesh with underneath Si wafer from the boundaries or breakages of graphene layer. As a consequence, the PCE decreases from 10.7% to 13.2% for small-area devices to 7.1–8.6% for larger-area devices (~ 30% relative drop). In spite of this, the PCE of 8.6% (for purple-color device) still represents the highest efficiency for 1 cm^2 Gr/Si heterojunction solar cells reported thus far.

To explore potential application of Gr/Si color solar cells, we further demonstrated a patterned color solar cell on a 2-in. Si wafer with two different colors, which shows the school badge of Soochow University (Fig. 6a). The golden region around the outside of the Si wafer is metal electrode (Au/Ag, 50 nm/50 nm) to form contact with graphene. The circular region in the center of the wafer is the Gr/Si junction area with DL-MgF_2/ZnS coating. Metal grid mesh electrode is used to enhance the conductivity of graphene layer. In this case, the text area is purple and the background is yellow. The pattern was formed by photolithography, while the colors were expressed by using DL-MgF_2/ZnS with different film thicknesses (purple: MgF_2/ZnS 120 nm/60 nm, yellow: MgF_2/ZnS 220 nm/130 nm). Interesting, the patterned Gr/Si heterojunction color solar cell can work well. The micro-field EQE spectra recorded from different areas are consistent with the colors and light absorptions in these areas. The lower absorption before 400 nm, corresponding to declined EQE value in the spectrum, results in the purple color in text area (Fig. 6b). Meanwhile, the weak absorption in the range of 550–750 nm leads to a yellow-green-color for the background area (Fig. 6c). It is noted that the hue deviation at background comes from the non-uniform film evaporation in large area. Such patterned color solar cells possess the potential to lead the way to a broad range of novel applications.

4. Conclusion

In summary, by synthetically considering the light absorption and reflection of Gr/Si heterojunction solar cells, we designed color Gr/Si solar cells by using DL-MgF_2/ZnS coating. The DL-MgF_2/ZnS films could effectively reduce the width of constructive interference peak in VIS, which was responsible for color development, while retaining minimizing parasitic reflection by other interference peaks. This strategy enabled the fabrication of Gr/Si solar cells with both high color saturation and high device performance. The multi-color DL-MgF_2/ZnS-coated Gr/Si solar cells exhibited a high PCE of 10.7–13.2%. Also, the

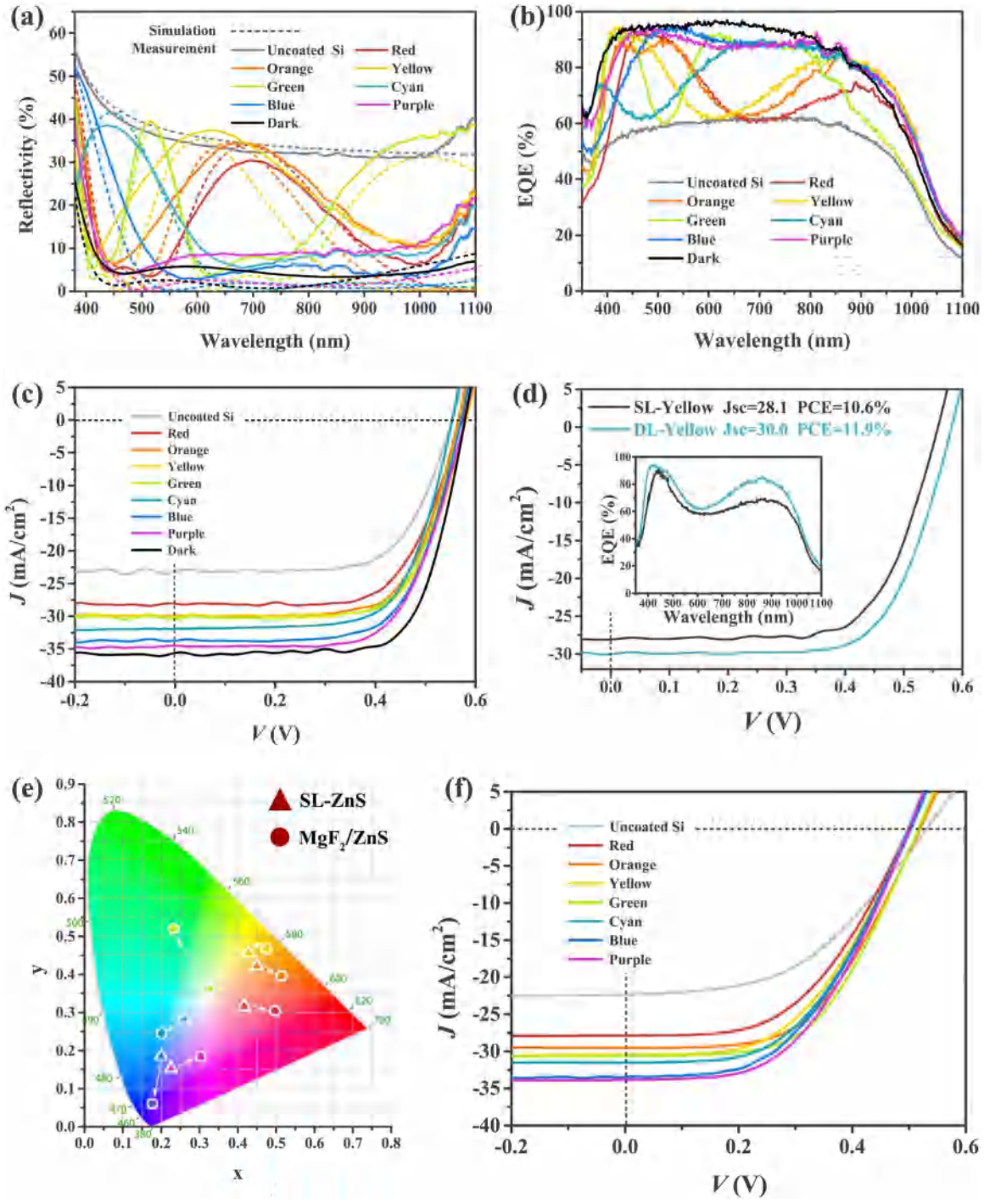

Fig. 5. (a) Reflection spectra of DL-MgF_2/ZnS-coated Gr/Si heterojunction solar cells with different structural colors obtained by optical measurements (solid lines) and simulation (dash lines) showing good agreements. The device areas for all the devices were fixed at 0.07 cm^2. (b) EQE spectra of the Gr/Si solar cells with different structural colors. EQE spectra of the device without coating and with optimized DL-MgF_2/ZnS anti-reflection coating were also presented for comparison. (c) *J-V* spectra of the devices with different structural colors measured under AM1.5, 100 mW/cm^2. *J-V* spectra of the devices without coating and with optimized anti-reflection coating were also presented for comparison. (d) Comparison of the *J-V* and EQE (inset) between SL-ZnS-coated and DL-MgF_2/ZnS-coated Gr/Si devices. (e) Comparison of color coordinates for SL-ZnS-coated and DL-MgF_2/ZnS-coated Gr/Si devices with different colors. The triangular and circle coordinate points represent the colors induced by SL-ZnS coating and DL-MgF_2/ZnS coating, respectively. (f) *J-V* curves of 1 cm^2 devices with different colors.

PCE of the device using optimized MgF_2/ZnS antireflection coating reached 14.6%. This is among the highest for Gr/Si heterojunction solar cells. By using a highly-transparent Ag grid mesh electrode to enhance the conductivity of graphene, the multi-color Gr/Si solar cells with large device area of 1 cm^2 was demonstrated. The PCE of 8.6% for purple-color device represented the best result for larger-area Gr/Si heterojunction solar cells. Eventually, a 2-in. Gr/Si solar cell with visible pattern was fabricated to explore the potential application of the multi-color Gr/Si solar cells. Our results pave the way toward the fabrication of color Gr/Si heterojunction solar cells for future low-cost, high-efficiency and designable PV panels.

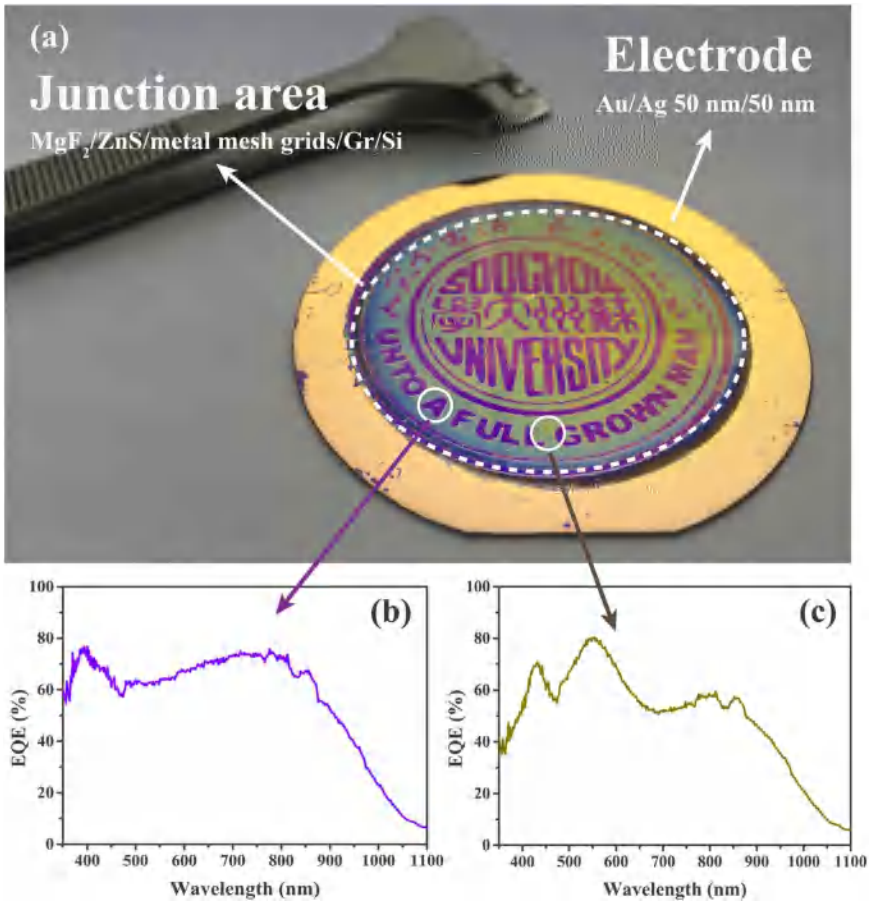

Fig. 6. (a) Photograph of the Gr/Si solar cell with visible graphics (school badge of Soochow University) on a 2-in. Si wafer. (b) and (c) show EQE spectra obtained at purple and yellow-green regions, respectively.

Acknowledgments

This work was supported by the National Basic Research Program of China (No. 2016YFA0202400), the National Natural Science Foundation of China (Nos. 61422403, 51672180, 51622306, 21673151), the China Postdoctoral Science Foundation (No. 2016M601880, 2017T100396), Collaborative Innovation Center of Suzhou Nano Science and Technology (NANO-CIC), and a Project Funded by the Priority Academic Program Development of Jiangsu Higher Education Institutions (PAPD).

Competing interests

The authors declare no competing financial interests.

Appendix A. Supporting information

Supplementary data associated with this article can be found in the online version at http://dx.doi.org/10.1016/j.nanoen.2018.02.005

References

[1] B.P. Jelle, C. Breivik, H.D. Rokenes, Sol. Energy Mater. Sol. Cells 100 (2012) 69.
[2] F.C. Krebs, N. Espinosa, M. Hosel, R.R. Sondergaard, M. Jorgensen, Adv. Mater. 26 (2014) 29.
[3] A. Fakharuddin, R. Jose, T.M. Brown, F. Fabregat-Santiago, J. Bisquert, Energy Environ. Sci. 7 (2014) 3952.
[4] J.H. Noh, S.H. Im, J.H. Heo, T.N. Mandal, S.I. Seok, Nano Lett. 13 (2013) 1764.
[5] H. Kim, J.P. Ge, J. Kim, S.-E. Choi, H. Lee, H. Lee, W. Park, Y.D. Yin, S. Kwon, Nat. Photonics 3 (2009) 534.
[6] T. Xu, H.F. Shi, Y.K. Wu, A.F. Kaplan, J.G. Ok, L.J. Guo, Small 7 (2011) 3128.
[7] S. Vignolini, P.J. Rudall, A.V. Rowland, A. Reed, E. Moyroud, R.B. Faden, J.J. Baumberg, B.J. Glover, U. Steiner, Proc. Natl. Acad. Sci. USA 109 (2012) 15712.
[8] Y.C. Shen, V. Rinnerbauer, I. Wang, V. Stelmakh, J.D. Joannopouos, M. Soljacic, ACS Photonics 2 (2015) 27.
[9] R.H. Muller, M.L. Sand, Appl. Opt. 26 (1987) 5211.
[10] H.J. Yang, C.H. Chen, W.C. Lai, C.L. Wu, C.F. Huang, Y.H. Chen, J.C. Hwang, J. Electrochem. Soc. 158 (2011) H851.
[11] I. Tobias, A. El Moussaoui, A. Luque, IEEE Trans. Electron. Dev. 46 (1999) 1858.
[12] M.H. Li, L.B. Zeng, Y.F. Chen, L. Zhuang, X.M. Wang, H. Shen, Int. J. Photoenergy 2013 (2013) 352473.
[13] J.H. Selj, T.T. Mongstad, R. Sondena, E.S. Marstein, Sol. Energy Mater. Sol. Cells 95 (2011) 2576.
[14] W. Zhang, M. Anaya, G. Lozano, M.E. Calvo, M.B. Johnston, H. Miguez, H.J. Snaith, Nano Lett. 15 (2015) 1698.
[15] A.G. Aberle, Prog. Photovolt. 8 (2000) 473.
[16] M. Taguchi, A. Yano, S. Tohoda, K. Matsuyama, Y. Nakamura, T. Nishiwaki, K. Fujita, E. Maruyama, IEEE J. Photovolt. 4 (2014) 96.
[17] R.Y. Liu, S.T. Lee, B.Q. Sun, Adv. Mater. 26 (2014) 6007.
[18] C. Xie, X.Z. Zhang, Y.M. Wu, X.J. Zhang, X.W. Zhang, Y. Wang, W.J. Zhang, P. Gao, Y.Y. Han, J.S. Jie, J. Mater. Chem. A 1 (2013) 8567.
[19] V.V. Brus, M.A. Gluba, X. Zhang, K. Hinrichs, J. Rappich, N.H. Nickel, Sol. Energy 107 (2014) 74.
[20] F. Bonaccorso, L. Colombo, G.H. Yu, M. Stoller, V. Tozzini, A.C. Ferrari, R.S. Ruoff, V. Pellegrini, Science 347 (2015) 1246501.
[21] X.M. Li, Z. Lv, H.W. Zhu, Adv. Mater. 27 (2015) 6549.
[22] X.M. Wang, Z.Z. Cheng, K. Xu, H.K. Tsang, J.B. Xu, Nat. Photonics 7 (2013) 888.
[23] Y. Song, X.M. Li, C. Mackin, X. Zhang, W.J. Fang, T. Palacios, H.W. Zhu, J. Kong, Nano Lett. 15 (2015) 2104.
[24] T. Yu, F. Wang, Y. Xu, L.L. Ma, X.D. Pi, D.R. Yang, Adv. Mater. 28 (2016) 4912.
[25] Z.F. Chen, X.M. Li, J.Q. Wang, L. Tao, M.Z. Long, S.J. Liang, L.K. Ang, C. Shu, H.K. Tsang, J.B. Xu, ACS Nano 11 (2017) 430.
[26] M.L. Tsai, W.C. Tu, L.B. Tang, T.C. Wei, W.R. Wei, S.P. Lau, L.J. Chen, J.H. He, Nano Lett. 16 (2016) 309.
[27] P.H. Ho, Y.T. Liou, C.H. Chuang, S.W. Lin, C.Y. Tseng, D.Y. Wang, C.C. Chen, W.Y. Hung, C.Y. Wen, C.W. Chen, Adv. Mater. 27 (2015) 1637.
[28] D.K. Xu, J. He, X.G. Yu, D.C. Gao, L.L. Ma, X.H. Mu, M.Y. Zhong, Y. Xu, J.C. Ye, M.S. Xu, D.R. Yang, Adv. Electron. Mater. 3 (2017) 1600516.
[29] A. Di Bartolomeo, G. Luongo, F. Giubileo, N. Funicello, G. Niu, T. Schroeder, M. Lisker, G. Lupina, 2D Material 4 (2017) 11.
[30] A. Di Bartolomeo, F. Giubileo, G. Luongo, L. Iemmo, N. Martucciello, G. Niu,

M. Fraschke, O. Skibitzki, T. Schroeder, G. Lupina, 2D Material 4 (2017) 11.
[31] K. Ding, X.J. Zhang, F.F. Xia, R.B. Wang, Y.W. Kuang, S. Duhm, J.S. Jie, X.H. Zhang, J. Mater. Chem. A 5 (2017) 285.
[32] S.L. Diao, X.J. Zhang, Z.B. Shao, K. Ding, J.S. Jie, X.H. Zhang, Nano Energy 31 (2017) 359.
[33] X.M. Li, H.W. Zhu, K.L. Wang, A.Y. Cao, J.Q. Wei, C.Y. Li, Y. Jia, Z. Li, X. Li, D.H. Wu, Adv. Mater. 22 (2010) 2743.
[34] C. Xie, X.J. Zhang, K.Q. Ruan, Z.B. Shao, S.S. Dhaliwal, L. Wang, Q. Zhang, X.W. Zhang, J.S. Jie, J. Mater. Chem. A 1 (2013) 15348.
[35] E.Z. Shi, H.B. Li, L. Yang, L.H. Zhang, Z. Li, P.X. Li, Y.Y. Shang, S.T. Wu, X.M. Li, J.Q. Wei, K.L. Wang, H.W. Zhu, D.H. Wu, Y. Fang, A.Y. Cao, Nano Lett. 13 (2013) 1776.
[36] L.J. Brillson, Surf. Sci. Rep. 2 (1982) 123.
[37] H. Haick, P.T. Hurley, A.I. Hochbaum, P.D. Yang, N.S. Lewis, J. Am. Chem. Soc. 128 (2006) 8990.
[38] A. Bansal, X.L. Li, I. Lauermann, N.S. Lewis, S.I. Yi, W.H. Weinberg, J. Am. Chem. Soc. 118 (1996) 7225.
[39] F.T. Zhang, B.Q. Sun, T. Song, X.L. Zhu, S.T. Lee, Chem. Mater. 23 (2011) 2084.
[40] L.N. He, C.Y. Jiang, H. Wang, D. Lai, Rusli, Appl. Phys. Lett. 100 (2012) 12344.

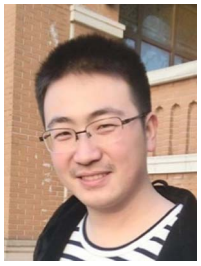

Ke Ding received his B.S. degree in Hefei University of Technology in 2013. He is currently a Ph.D. student in Institute of Functional Nano & Soft Materials (FUNSOM), Soochow University. His research mainly focus on the silicon based heterojunction solar cells.

Xiujuan Zhang received her Ph.D. degree in chemistry from Technical Institute of Physics and Chemistry, Chinese Academy of Sciences (CAS) in 2006. After that, she worked as a postdoctoral fellow at City University of Hong Kong. In 2009, she joined institute of Functional Nano & Soft Materials (FUNSOM), Soochow University. Her research involves design and synthesis of semiconductor nanostructure and their applications in optoelectronic devices.

Ling Ning is currently a graduate student in the institute of Functional Nano & Soft Materials (FUNSOM), Soochow University. She received her B.S. degree in the College of Physics, Optoelectronics and Energy of Soochow University in 2015. Her research mainly focus on two dementional materials based optoelectronic devices.

Zhibin Shao received his B.S. and Ph.D. degree in physics from University of Science and Technology of China (USTC) in 2007 and 2013, respectively. After that, he joined institute of Functional Nano & Soft Materials (FUNSOM), Soochow University. His research involves the surface charge transfer doping (SCTD) of low-dimensional nanostructures and their application in opto/electronic nanodevices.

Peng Xiao received his B.S. degree from Jiangsu University of Science and Technology In 2010. He is currently a Ph.D. candidate in Institute of Functional Nano & Soft Materials (FUNSOM), Soochow University. His research interests mainly focused on 2D materials/Si heterojunctions applied in photovoltaic and optoelectronic devices.

Anita Ho-Baillie received her B.E. and Ph.D. degree at The University of New South Wales (UNSW) in 2001 and 2005, respectively. She worked as deputy director in Australian Research Council (ARC) Center of Excellence for Photovoltaics from 2002 to 2009. After that, she worked in Solar Sailor Holdings Ltd. until 2010. In 2010, she joined the School of Photovoltaic and Renewable Energy Engineering, UNSW. She is also the Program Manager for the Perovskite Solar Cell Research at the Australian Center for Advanced Photovoltaics.

Xiaohong Zhang received his B.S. and M.S. degree at Beihang University in 1989 and 1992, respectively. He obtained his Ph. D. degree at Beijing Institute of Technology in 1996. After that, he worked as post-doctor at Institute of Photographic Chemistry of Chinese Academy of Sciences (CAS), and City University of Hong Kong respectively. He joined Technical Institute of Physics and Chemistry of CAS as a professor in 2000. Since 2013, he came to Institute of Functional Nano & Soft Materials (FUNSOM), Soochow University, as a professor. His research interests include organic optoelectronic materials, semiconductor nanomaterials and optoelectronic devices.

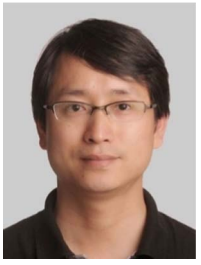

Jiansheng Jie received his B.S. and Ph.D. degree in physics from University of Science and Technology of China in 1999 and 2004 respectively. He then worked as a postdoctoral fellow at the City University of Hong Kong. After that, he came to work at Hefei University of Technology at 2006 as a professor. In 2010, he joined Institute of Functional Nano & Soft Materials, Soochow University. His research focuses on the synthesis of organic and inorganic nanostructures for their flexible electronics, optoelectronics, and solar energy conversion devices.